ONCOIMMUNOLOGY
2022, VOL. 11, NO. 1, e2144669 (15 pages)
https://doi.org/10.1080/2162402X.2022.2144669

Taylor & Francis
Taylor & Francis Group

ORIGINAL RESEARCH

OPEN ACCESS Check for updates

Chemokine switch regulated by TGF-β1 in cancer-associated fibroblast subsets determines the efficacy of chemo-immunotherapy

Angélique Vienot[a,b,c], Jean-René Pallandre[b], Elodie Renaude[b], Julien Viot[a,b], Adeline Bouard[b,d], Laurie Spehner[b], Marie Kroemer[b,d], Syrine Abdeljaoued[b], Bas van der Woning[e], Hans de Haard[e], Romain Loyon[b], Eric Hervouet[b,f], Paul Peixoto[b,f], and Christophe Borg[a,b,c,d]

[a]Department of Medical Oncology, University Hospital of Besançon, F-25000 Besançon, France; [b]INSERM, EFS BFC, UMR1098, RIGHT, University of Bourgogne Franche-Comté, Interactions Greffon-Hôte-Tumeur/Ingénierie Cellulaire et Génique, F-25000 Besançon, France; [c]Clinical Investigational Center, CIC-1431, F-25000 Besançon, France; [d]ITAC platform, University of Bourgogne Franche-Comté, F-25000 Besançon, France; [e]Argenx, 9052 Zwijnaarde, Belgium; [f]EPIgenetics and GENe EXPression Technical Platform (EPIGENExp), University of Bourgogne Franche-Comté, F-25000 Besançon, France

ABSTRACT

Combining immunogenic cell death-inducing chemotherapies and PD-1 blockade can generate remarkable tumor responses. It is now well established that TGF-β1 signaling is a major component of treatment resistance and contributes to the cancer-related immunosuppressive microenvironment. However, whether TGF-β1 remains an obstacle to immune checkpoint inhibitor efficacy when immunotherapy is combined with chemotherapy is still to be determined. Several syngeneic murine models were used to investigate the role of TGF-β1 neutralization on the combinations of immunogenic chemotherapy (FOLFOX: 5-fluorouracil and oxaliplatin) and anti-PD-1. Cancer-associated fibroblasts (CAF) and immune cells were isolated from CT26 and PancOH7 tumor-bearing mice treated with FOLFOX, anti-PD-1 ± anti-TGF-β1 for bulk and single cell RNA sequencing and characterization. We showed that TGF-β1 neutralization promotes the therapeutic efficacy of FOLFOX and anti-PD-1 combination and induces the recruitment of antigen-specific $CD8^+$ T cells into the tumor. TGF-β1 neutralization is required in addition to chemo-immunotherapy to promote inflammatory CAF infiltration, a chemokine production switch in CAF leading to decreased CXCL14 and increased CXCL9/10 production and subsequent antigen-specific T cell recruitment. The immune-suppressive effect of TGF-β1 involves an epigenetic mechanism with chromatin remodeling of CXCL9 and CXCL10 promoters within CAF DNA in a G9a and EZH2-dependent fashion. Our results strengthen the role of TGF-β1 in the organization of a tumor microenvironment enriched in myofibroblasts where chromatin remodeling prevents CXCL9/10 production and limits the efficacy of chemo-immunotherapy.

ARTICLE HISTORY
Received 8 May 2022
Revised 2 November 2022
Accepted 2 November 2022

KEYWORDS
fibroblast; TGF-β; chemo-immunotherapy; chemokine; cancer; microenvironment

Introduction

Combining immunogenic cell death (ICD)-inducing chemotherapies with inhibitory immune checkpoint blockade is a promising therapeutic approach developed in several malignancies. If a growing number of patients will be treated by chemo-immunotherapy in a near future, the cellular and molecular determinants limiting the efficacy of this combination need to be fully explored. Transforming growth factor-β1 (TGF-β1) contributes to avoiding tumor infiltration by T cells and decreases the efficacy of anti-programmed cell death (ligand) 1 (PD-1/L1) treatments.[1–3] However, TGF-β1 and PD-L1 dual blockade provide moderate clinical efficacy in early clinical research.[4,5] In cancer models with low tumor infiltration and barely sensitive to immunotherapy, immune checkpoint inhibitors (ICI) efficacy may be enhanced by the potential immunogenic effects of cytotoxic chemotherapy.[6–9] The implication of TGF-β1 in the resistance mechanisms limiting the activity of chemo-immunotherapy remains to be fully investigated.

Several molecular classifications of colorectal cancers (CRC) have consistently shown that TGF-β1 transcriptional activity and infiltration by cancer-associated fibroblasts (CAF) cooperate to dictate poor clinical outcomes.[10,11] Pan-cancer analyses also established the presence of a TGF-β1-associated stromal signature correlated with immunotherapy failure and independent of tumor types.[12] Bulk RNA-sequencing (RNA-seq) analyses contributed to deciphering molecular pathways involved in TGF-β1 mediated immunosuppression. A signature related to TGF-β1 and stroma expression was associated with $CD8^+$ T cell exclusion and the lack of response in urothelial cancer patients treated with ICI targeting PD-L1.[1]

CAF constitute a heterogeneous tumor microenvironment (TME) cell type consisting of various subpopulations, including myofibroblastic CAF (myCAF) and a population of CAF secreting inflammatory cytokines such as IL-6 (iCAF).[13] myCAF differentiate in the presence of TGF-β1 and are characterized by αSMA expression.[13–17] While myCAF and iCAF coexist as two reversible subtypes, both CAF subsets exert

CONTACT Angélique Vienot a3vienot@chu-besancon.fr Department of Medical Oncology, University Hospital of Besançon, INSERM UMR1098, EFS Bourgogne Franche-Comté, 3 Boulevard Alexandre Fleming, 25030 Besançon, France
Supplemental data for this article can be accessed online at https://doi.org/10.1080/2162402X.2022.2144669

tumor-promoting and tumor-restraining functions.[13,18] Production of Th1-type chemokines (CXCL9 and CXCL10) determines effector T cell tumor infiltration, in response to interferon-γ (IFNγ) induced by ICI.[19] It has been previously described that TGF-β1 neutralization combined with anti-PD -1 immunotherapy correlates *in vivo* with the presence of a subset of CAF an optimal biological level of IFN response.[20] The role of TGF-β1 in remodeling CAF subsets and functions has not been investigated when ICD-inducing chemotherapy is combined with immunotherapy.

Here, we conducted a research program, using several syngeneic murine models of colon and pancreatic cancers, to explore how TGF-β1 modulates chemokine production within CAF subpopulations during chemo-immunotherapy. We first demonstrated that TGF-β1 represses tumor-reactive $CD8^+$ cell infiltration and CXCL9/10 expression in CAF. Using single-cell RNA-seq (scRNA-seq), we revealed that TGF-β1 controls the diversity of CAF subsets during chemo-immunotherapy. TGF-β1 signaling restrains tumor infiltration by iCAF while promoting the presence of the myCAF subset. TGF-β1 mediated chromatin remodeling prevents CXCL9/CXCL10 expression by fibroblasts in a G9a and EZH2-dependent fashion.

Materials and methods

Cell lines

CT26 colon cancer cells, 4T1 mammary breast cancer cells, and NIH/3T3 fibroblasts were purchased from ATCC (CRL-2638, CRL-2539, and CRL-1658, respectively; ATCC American Type Culture Collection, Manassas, VA). MC-38 colon cancer cells were purchased from Kerafast (ENH204-FP). PancOH7 pancreatic cancer cells were kindly provided by Pr. Panigrahy D. (Beth Israel Deaconess Medical Center, Boston, USA). CT26 and 4T1 cell lines were cultured in Roswell Park Memorial Institute medium (RPMI 1640) supplemented with 10% heat inactivated fetal calf serum and 1% of penicillin-streptomycin (Gibco). NIH/3T3, PancOH7, and MC-38 cell lines were cultured in Dulbecco's Modified Eagle Medium (DMEM; Gibco) supplemented with 10% heat inactivated fetal calf serum and 1% of penicillin-streptomycin (Gibco). All cell lines were routinely tested for *Mycoplasma* by PCR assays.

Generation of mice tumor models

Female C57BL/6JRj and BALB/cByJRj mice were purchased from Center d'élevage Janvier (Le Genest St Isle, France). For *in vivo* animal studies, mice were 6–8 weeks old. All experimental studies were approved by the local ethics committee following the European Union's Directive 2010/63. Only animals that appeared to be healthy and free of obvious abnormalities were used for studies. Mice were inoculated subcutaneously in the right flank with 2.10^5 CT26, 5.10^5 PancOH7, 2.10^5 MC-38, or 2.10^5 4T1 cells in 100 µl of phosphate-buffered saline (PBS, Gibco). Tumor growth was monitored twice a week with a caliper. Mice were randomized and treated in five groups when tumor size reached 50–60 mm^3.

C57BL/6J $FAP^{-/-}$ mice (Stock No: 024288 B6;129P2-Faptm2Schn/J) were obtained from Jackson Laboratory, USA. BALB/cByJ $FAP^{-/-}$ were generated by crossing C57BL/6J $FAP^{-/-}$ with BALB/cByJ wild-type mice for more than eight generations. The genotype of BALB/c $FAP^{-/-}$ mice generated was validated by PCR assays.

37–44 days after tumor implantation or when tumors exceeded 1500 mm^3 (due to ethical reasons), mice were euthanized. Survival curves were plotted, and tumors were collected for either flow cytometry analysis, enzyme-linked immunosorbent assay (ELISA), RT-qPCR, bulk or single-cell RNA-seq.

Treatments

All chemotherapy procedures were conducted in the Department of Pharmacy, University Hospital of Besançon (France). FOLFOX regimen was administered with an intraperitoneal (IP) single dose of 5-fluorouracil (50 mg/kg) and oxaliplatin (6 mg/kg). The control group received the solvent used to dilute the drug and the appropriate isotype antibodies anti-rat IgG2a (2A3, Euromedex) and anti-mouse IgG1 (MOPC-21, Euromedex). Anti-PD-1 (RMP1-14, Euromedex) and anti-TGF-β1 (1D11, Euromedex) mouse antibodies IP injections were started concomitantly with the chemotherapy treatment: 200 µg per mouse twice a week for two weeks.

Tumor re-challenge, Treg and T cell depletion experiments

For tumor re-challenge experiments, naïve and tumor-free mice were inoculated subcutaneously with 2.10^5 4T1 cells in the left flank and with 2.10^5 CT26 cells in the right flank. FOXP3-DTR-GFP mice were injected subcutaneously with 5.10^5 PancOH7 cells in 100 µl of PBS. Mice were randomized and treated in four groups when tumor size reached 50–60 mm^3. For Treg depletion, diphtheria toxin (DT; Sigma-Aldrich, France) was administered with an IP dose at 50 µg/kg, diluted in PBS, per week for two weeks. The first injection of DT was performed one day before all other treatments, when the tumor size of mice reached 50–60 mm^3. For $CD8^+$ T cells depletion experiments, an anti-CD8 antibody (YTS 169.4, Euromedex) was administered IP once at 500 µg per mouse.

Tumor digestion and cell isolation

For the preparation of cell suspensions, subcutaneous tumors were collected and finely minced with sterile scissors. Tumor fragments were enzymatically and mechanically digested using Tumor dissociation kit mouse (Miltenyi) with gentleMACS dissociator for 45 minutes at 37°C. Following tumor digestion, cells were passed through a 70-µm nylon cell strainer and resuspended in flow cytometry buffer (PBS, 2% FBS with 2 mM EDTA). Cells were separated using magnetic microbeads for immune cells (CD45 MicroBeads, Miltenyi) $CD4^+$ T cells (CD4 MicroBeads mouse, Miltenyi), macrophages (CD11b MicroBeads mouse, Miltenyi), endothelial cells (CD31 MicroBeads mouse, Miltenyi), and fibroblasts (Tumor Associated Fibroblast Isolation kit mouse, Miltenyi) populations. The quality of magnetic cell sorting was evaluated by FACS with fluorophore-conjugated antibodies purchased from

Sony Biotechnology (UK): CD45 (30-F11), CD4 (GK1.5), CD8a (53–6.7), CD11b (M1/70), CD31 (390), CD90.2 (30-H12).

Cell culture and epigenetic treatment

Fibroblasts were isolated from the skin derived from ears of C57BL/6JRj naïve mice after digestion by collagenase P for 60 minutes at 37°C. After tissue digestion, cells were filtered and cultured in a petri dish in DMEM with FBS 10%. For TGF-β1 treatment, fibroblasts were incubated with 10 ng/mL TGF-β1 (Peprotech) for 48 hours before treatment with 20 ng/mL IFNγ (Peprotech) for 24 hours. Fibroblasts were pretreated with 5 µM EZH2 inhibitor (GSK343; Sigma Aldrich), 0.5 µM G9a inhibitor (UNC0638; Sigma Aldrich), or 5 µM JMJD3/KDM6B and UTX/KDM6A inhibitor (GSKJ4; Sigma Aldrich) for three days before TGF-β1 treatment with or without restimulation by IFNγ. Fibroblasts were used between passages 3–6 for all experiments: ELISA, RT-qPCR, chromatin immunoprecipitation (ChIP), and bulk RNA-seq.

Small interfering RNA (siRNA) transfection

Naive fibroblasts were transfected with siRNA against mouse EZH2 (5'-CAGACGAGCTGATGAAGTAAA-3') or mouse G9a (5'-CACCATGAACATCGACCGCAA-3') (Genecust) using TransIT-X2 Transfection Reagent (Mirus) according to the manufacturer's instructions. After 72 hours of transfection, cells were exposed to TGF-β1 treatment (10 ng/mL for 48 hours) with or without restimulation by IFN-γ (20 ng/mL for 24 hours).

Chromatin immunoprecipitation (ChIP)

Chromatin was prepared with the truChIP™ Chromatin Shearing Kit (Covaris) according to the manufacturer's instructions. Each sample was sonicated for 15 min using Covaris E220 sonicator. ChIP were performed using the IP-Star Compact Automated System (Diagenode). One µg of isolated chromatin was immunoprecipitated with 1.6 µg of anti-Histone H3 lysine 9 trimethylation (H3K9me3) (ab8898, Abcam), 1.6 µg of anti-H3K9/K14ac (C15410200, Diagenode), 1.6 µg of anti-H3K27me3 (C15410069, Diagenode) or 1.6 µg of IgG (PP64B, Millipore) in dilution buffer (0.01% SDS; 1.1% Triton X 100; 2 mM EDTA; 16.7 mM Tris-Cl pH 8.0; 167 mM NaCl; 1× protease inhibitor cocktail, Sigma Aldrich). The DNA/protein complexes were washed two times in IP Wash buffer 1 (20 mM Tris-HCl pH 8.0; 0.1% SDS; 1% Triton X-100; 2 mM EDTA; 150 mM NaCl) and two times in IP Wash buffer 2 (20 mM Tris-HCl pH8; 0.1% SDS; 1% Triton X-100; 2 mM EDTA, 450 mM NaCl). After reversal of cross-linking, the immunoprecipitated DNA was purified using Chromatin IP DNA Purification kit (Active Motif) and analyzed employing RT-qPCR with the SYBR-Green Takara (Ozyme) and step one plus applied Real-Time PCR system. For CXCL9 and CXCL10 promoters amplification, the following primers were used: CXCL9 forward (5′-TGGAAAAGGTAGCAGGGAAC−3′), reverse (5'-CGACTCAAACTGCCTTTCCT−3′), and CXCL10 forward (5'-GGCTAAATTTGGCGTGTGAT−3′), reverse (5′-TGCAGTGCCTTGCAGAATAA−3′). PCR was performed with initial denaturation of 10 minutes at 95°C, followed by 45 cycles of 10 seconds at 95°C, 30 seconds at 60°C, and 30 seconds at 72°C.

Single-cell RNA-sequencing

For scRNA-seq, C57BL6 mice with PancOH7 tumors treated with FOLFOX, anti-PD-1 ± anti-TGF-β1 (four in each condition) were sacrificed two days after the last antibodies injection. Single-cell suspensions were isolated as described above from tumor-bearing mice. Cells were separated by magnetic cell sorting for immune cells and fibroblasts populations, and up to 12,000 cells (4,000 $CD45^+$ and 8,000 CAF) from each sample were loaded per lane on 10X Genomics Chromium microfluidic chips. Single-cell capture, barcoding, and library preparation were performed using the 10X Genomics Chromium™ version 3 chemistry, according to the manufacturer's protocol (10X Genomics). cDNA and final libraries were checked using the Bioanalyzer High Sensitivity DNA Kit (Agilent Technologies). Each scRNA-seq library was sequenced on an Illumina HiSeq 4000 using paired-end 2×100 bp lanes sequencing.

Statistical analyses

Median value (interquartile range) and frequency (percentage) were provided for the description of continuous and categorical variables, respectively. Medians were compared using Wilcoxon-Mann-Whitney or Kruskal-Wallis, and proportions were compared using chi-square tests (or Fisher's exact test, if appropriate). Pearson's test was applied to determine the correlation between gene or signature expressions. Overall survival (OS) was estimated using the Kaplan-Meier method and described using median or rate at specific time points with 95% confidence intervals (CI), and compared using the log-rank test. All analyses were performed using GraphPad version 8.1.2 (GraphPad software, USA) and R software version 3.5.3 (R Development Core Team, Austria; http://www.r-project.org). All tests were two-sided and p-values of less than .05 were considered statistically significant.

Data Availability

All data generated or analyzed during this study are available within the article and its supplementary information files and from the corresponding author upon reasonable request. More detailed information is available in the online supplemental material section.

Results

TGF-β1 neutralization promotes therapeutic efficacy of FOLFOX and anti-PD-1 combination

In order to better understand the potential obstacle to ICD-inducing chemotherapy and anti-PD-1 combination, we selected preclinical models where immunotherapies targeting anti-PD-1 ± anti-TGF-β1 were not effective in monotherapy or in combination (Figure S1A). Although, addition of FOLFOX

to anti-PD-1 decreased the growth kinetics of CT26 and PancOH7 tumors, the combination did not generate complete tumor regression (Figure S1A).

We first sought to quantify by flow cytometry the proportion of tumor-infiltrating lymphocytes (TIL) in CT26 tumor-bearing mice exposed to immunogenic chemotherapy (FOLFOX) and anti-PD-1. Similar experiments were reproduced in the pancreatic model PancOH7 cell line which is endowed with the capacity to recruit fibroblasts and displaying a high metastatic potential. Treatment with FOLFOX failed to increase the intra-tumoral number of $CD3^+$ T cells in both models. Addition of anti-PD-1 barely increased percentages of intra-tumoral $CD8^+$ and regulatory T cells (Treg) in CT26 ($p = .06$) but not in PancOH7-bearing mice (Figure 1a). Nevertheless, the absolute number of $CD8^+$ T cells was not enhanced when PD-1 blockade was added to chemotherapy. Since TGF-β1 production is a possible mechanism accounting for tumor immune evasion, TGF-β1 levels were measured in tumor lysate from CT26 and PancOH7 tumor-bearing mice exposed to FOLFOX ± anti-PD-1. Even if chemo-immunotherapy decreased significantly TGF-β1 protein expression in both CT26 and PancOH7 whole tumor lysate ($p < .0001$), TGF-β1 levels remained high (>200 pg/mL; Figure 1b).[21,22]

We next addressed if TGF-β1 could be a limiting factor for FOLFOX+anti-PD-1 efficacy. For this purpose, previous experiments were reproduced in syngeneic models. Mice were treated with FOLFOX, anti-PD-1, and TGF-β1 inhibitor (Figure 1c). TGF-β1 inhibition did not improve FOLFOX efficacy (Figure 1d-e). However, the addition of neutralizing anti-TGF-β1 to chemo-immunotherapy led to significant tumor shrinkage compared to all other groups. These results were confirmed in MC-38 and 4T1 models (Figure S2). Overall, the objective response rate (ORR) observed across all experiments was over 85% in both models where TGF-β1 blockade was added to chemo-immunotherapy (56.7% vs 86.7%, $p < .01$ in CT26 model; 52.9% vs 88.2%, $p = .02$ in PancOH7 model). In addition, TGF-β1 blockade enabled durable complete responses (16.7% vs 46.7%; 23.5% vs 41.2% in CT26 and PancOH7 tumor-bearing mice treated with FOLFOX+anti-PD-1 with or without anti-TGF-β1; Figures 1d-e & S1B). Since Treg activation in tumors exposed to FOLFOX + PD-1 blockade might contribute to TGF-β1 suppressive functions, PancOH7 model treated with FOLFOX ± anti-PD-1 ± anti-TGF-β1 was reproduced in FOXP3-DTR (diphtheria toxin receptor) mice. TGF-β1 neutralization improved the efficacy of FOLFOX +anti-PD-1 even in Treg-depleted mice suggesting that the impact of TGF-β1 neutralization does not only rely on Treg inhibition (Figures 1f & S1C).

Altogether, these experiments support the role of TGF-β1 signaling as a resistance mechanism when ICD-inducing chemotherapy is combined with PD-1 blockade. The addition of TGF-β1 neutralization to chemo-immunotherapy is pivotal to achieving sustained complete remissions in these models.

TGF-β1 prevents the ability of chemo-immunotherapy to induce the recruitment of antigen-specific $CD8^+$ T cells into the tumor

The role of $CD8^+$ T cells in the complete remission observed when FOLFOX was combined with TGF-β1 and PD-1 dual blockade was investigated in $CD8^+$ lymphocytes depleted mice. $CD8^+$ T cell depletion prevented the impact of TGF-β1 inhibition in mice treated with FOLFOX+anti-PD-1 (Figure 2a). These results confirmed that the anti-tumor response potentiated by TGF-β1 neutralization requires $CD8^+$ T cells. To better understand how TGF-β1 signaling influences the cancer immune contexture during chemo-immunotherapy, TIL phenotype in the CT26 model was explored. Intra-tumoral $CD8^+$ T cell counts were significantly increased only in tumors treated with chemo-immunotherapy and TGF-β1 inhibitor ($p < .0001$). The effector functions of these lymphocytes were also enhanced as characterized by high levels of IFNγ and GzmB (Figure 2b). Similar observations were highlighted in PancOH7 and MC-38 models (Figure S3).

The murine endogenous tumor antigen gp70 allows the recognition of CT26-specific lymphocytes.[23] TGF-β1 neutralization promoted an enrichment of antigen-specific $CD8^+$ T cells in CT26 tumors as shown by gp70 tetramer staining (Figure 2c). Besides, $gp70^+IFN\gamma^+GzmB^+CD8^+$ T cells were only identified in tumors treated by chemo-immunotherapy and TGF-β1 inhibition (Figure 2d). Thus, TGF-β1 exerts an important suppressive activity to control specific $CD8^+$ lymphocyte infiltration and activation in cancer models when ICD-inducing chemotherapies are combined with anti-PD-1.

Moreover, CT26 tumor-bearing mice exposed to chemo-immunotherapy in previous experiments and achieving a complete remission were re-challenged with CT26 or an unrelated breast cancer cell line (4T1). All mice previously treated with FOLFOX, anti-PD-1, and anti-TGF-β1 combination rejected CT26 but not 4T1 suggesting that immunological memory against prior antigens can persist (Figure 2e).

TGF-β1 controls a CXCL9/10 and CXCL14 production switch in CAF exposed to chemo-immunotherapy

Chemokines guide the migration of immune cells and play a major role in the TME regulation. The production of Th1-type chemokines is associated with a T-cell-inflamed phenotype and CXCL9/10 are biomarkers of clinical response to anti-PD-1.[19,24] In contrast, CXCL14 is a chemoattractant for immature dendritic cells, monocytes, macrophages, and NK cells, but not T cells.[25] Chemokine levels were measured in whole tumor lysates by ELISA. Interestingly, while immunotherapy targeting PD-1 and TGF-β1 did not modulate CXCL9/10, TGF-β1 neutralization promoted the production of these two chemokines by the CT26 microenvironment following treatment with chemo-immunotherapy. Conversely, the CXCL14 level decreased after chemo-immunotherapy and anti-TGF-β1 (Figure 3a). Of note, we observed that FOLFOX induced CXCL14 production. The regulation of CXCL9/10/14 expression by TGF-β1 signaling in tumors was also confirmed by reverse transcription quantitative polymerase chain reaction (RT-qPCR; Figure S4A).

Tumor as well as TME cells ($CD4^+$ T cells, macrophages, endothelial cells, or CAF) can produce chemokines in response to cytokine stimulation. After tumor dissociation from the CT26 model, TME cells were isolated before bulk RNA-seq of each cell subtype exposed to chemo-immunotherapy ± anti-TGF-β1 (Figure S4B). TGF-β1 blockade led to an enhanced gene transcription modulation in fibroblasts compared to other

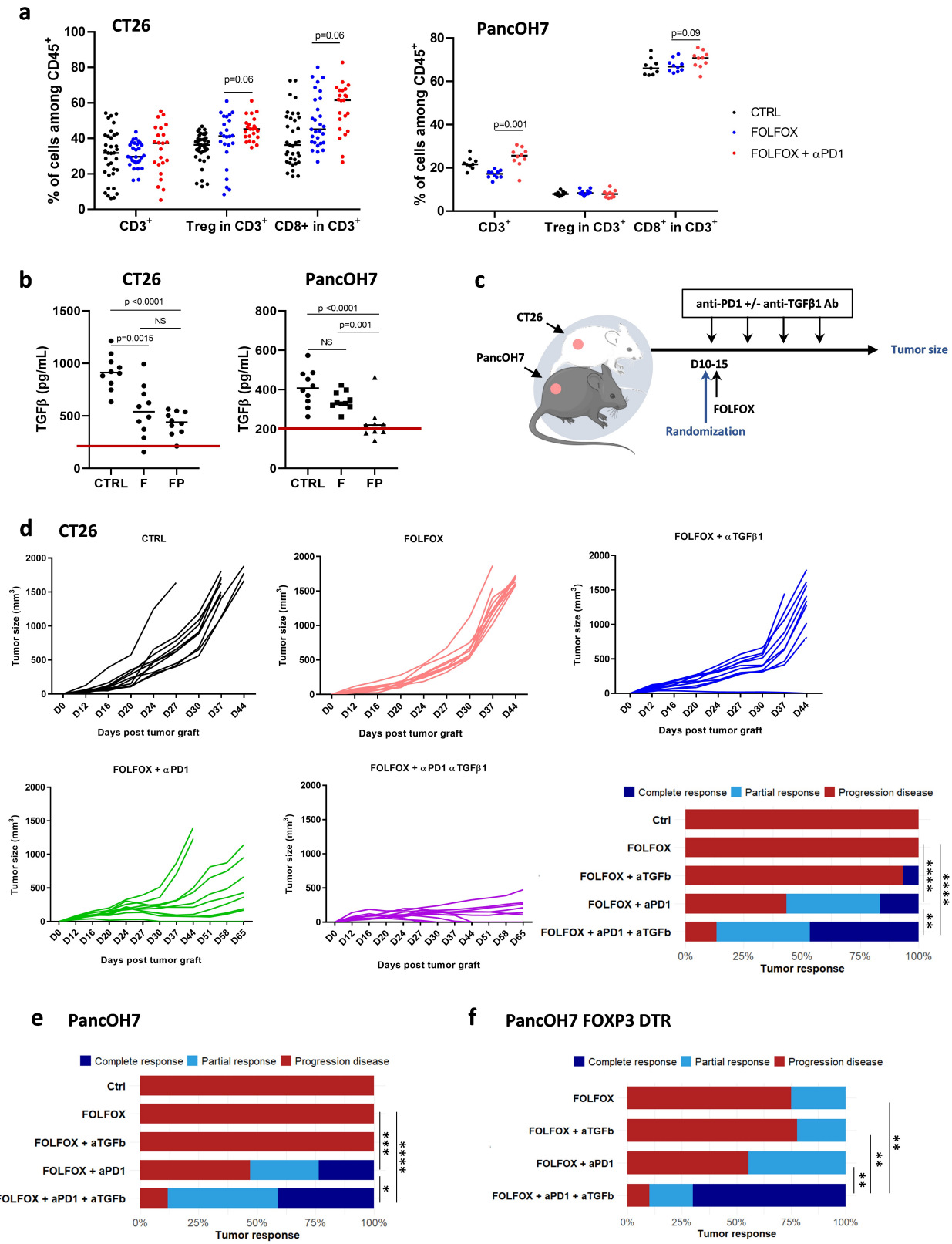

Figure 1. Adding TGF-β1 blockade to chemo-immunotherapy promotes complete tumor regression in CT26 and PancOH7 models. (a) Proportion of $CD3^+$, Treg, and $CD8^+$ T cells measured by flow cytometry in total $CD45^+$ intra-tumoral cells isolated from CT26 and PancOH7-bearing BALB/c and C57BL/6 mice, respectively. For this purpose, tumors were collected two days following the last treatment injection. (b) TGF-β1 levels determined in whole tumor lysate derived from CT26 and PancOH7-bearing mice after FOLFOX ± anti-PD-1 and measured by ELISA. Pooled results from two independent experiments are presented. Red line shows the threshold at 200 pg/mL. (c) Experimental scheme: BALB/c and C57BL/6 mice were injected subcutaneously with PancOH7 pancreatic tumor cells and CT26 colon tumor cells, respectively (five experiments in the CT26 model and three experiments in the PancOH7 model). Mice were randomized and treated in five groups (n = 5–10 per group) when tumor size reached 50–60 mm^3: Control, FOLFOX, FOLFOX +anti-TGF-β1, FOLFOX+anti-PD-1, and FOLFOX+anti-PD-1+ anti-TGF-β1. (d) Tumor growth and responses according to treatment groups for CT26 tumor-bearing mice. Tumor growths are indicated for one of a representative experiment, each line represents an individual mouse tumor size. Objective responses are shown for pooled mice (n = 30 per group). (e) Objective responses are shown in PancOH7 models for pooled C57BL/6 mice (n = 17 per group). (f) Objective responses are shown in PancOH7 models for pooled C57BL/6 FOXP3 DTR (diphtheria toxin receptor) mice (n = 10 in FPT group, n = 9 in other groups) for the depletion of regulatory T cells. *p ≤ .05 **p ≤ .01 ***p ≤ .001 ****p ≤ .0001. Abbreviations: Ab: antibody; Ctrl: control; F: FOLFOX; FP: FOLFOX+anti-PD-1.

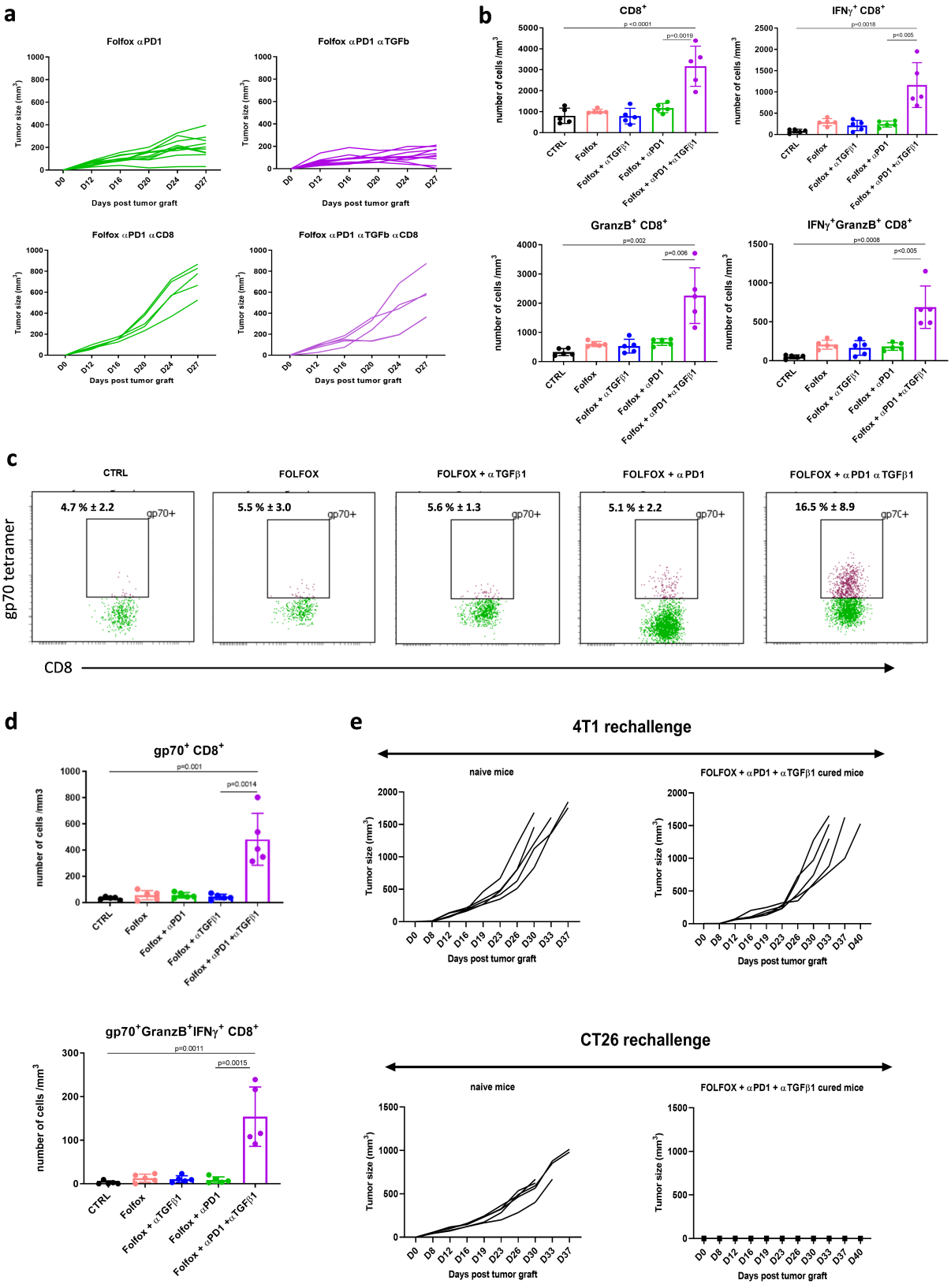

Figure 2. Adding TGF-β1 blockade to chemo-immunotherapy increases effector and specific T cell infiltration in the CT26 model. (a) Tumor growth in mice treated with FOLFOX, anti-PD-1 ± anti-TGF-β1, according to depletion of $CD8^+$ T lymphocytes. One representative experiments is shown (n = 3) (b) Numbers per mm^3 of total $CD8^+$ T cells (top left), IFNγ (Top right), GzmB (bottom left), and IFNγ/GzmB (Bottom right) expressing $CD8^+$ tumor-infiltrating lymphocytes (TIL), according to the five groups of treatment. One representative experiment out of 5 is depicted. (c) Representative flow cytometry dot plot graphs on AH1 specific $CD8^+$ TIL with gp70 tetramer staining. (d) Numbers per mm^3 of $gp70^+IFNγ^+GzmB^+$ expressing $CD8^+$ TIL. (e) Tumor growth of untreated or FOLFOX + anti-TGF-β1/PD-1-treated cured mice re-challenged with 4T1 (Top) and CT26 (Bottom) tumor cells, two months after previous treatment. Each experiment was repeated independently a minimum of three times in the same conditions.

TME cells (Figure 3b & Table S1). High CXCL9/10 and CXCL14 expression were observed in CAF, but low levels and modulation were observed in $CD4^+$ lymphocytes, macrophages, and endothelial cells (Figure 3c). Furthermore, a chemokine switch was only highlighted in CAF: CXCL9/10 were overexpressed following TGF-β1 inhibition, while CXCL14 was downregulated (Figure 3c). Of note, upregulated genes in the context of TGF-β1 blockade were strongly enriched for chemokine signaling (p-adjusted = .017, NES = 2.3; Figure S3C). The regulation of CXCL9/10/14 expression by TGF-β1 signaling in CAF was also confirmed by RT-qPCR in all models (CT26, PancOH7, MC-38, and 4T1; Figures 3d & S5). These results demonstrated that TGF-β1 drives a selective mechanism controlling CXCR3 ligand expression in CAF. The predominant role of CAF was highlighted since previous results were not reproduced in FAP knockout mice. TGF-β1 was not required for the anti-tumor efficacy of ICD-inducing chemotherapy and anti-PD-1 in $FAP^{-/-}$ mice (Figure S6). These results suggest that TGF-β1 might be a limiting factor for chemo-immunotherapy efficiency in desmoplasic tumors where CAF exert tumor-promoting functions.

TGF-β1 modulation reshapes cellular content in the microenvironment of tumors treated by chemo-immunotherapy

In previous studies, several CAF subsets were identified in human breast cancer or pancreatic ductal adenocarcinoma (PDAC) and were associated with immunosuppressive microenvironment or immunotherapy resistance.[15,26] To explore the influence of TGF-β1 neutralization on CAF heterogeneity, scRNA-seq analyses were conducted on CAF and $CD45^+$ hematopoietic cells from tumor-bearing mice treated with chemo-immunotherapy ± anti-TGF-β1. Four animals were pooled per condition and executed in two biological replicates. We first analyzed 11,975 viable cells with a median of expressed genes per cell of 1,962 (Figure S7A). t-distributed stochastic neighbor embedding (tSNE) projection allowed to distinguish 13 clusters, among which two clusters of contaminating cells: endothelial cells (cluster 9: *Plvap, Pecam1*, and *Cdh5*) and tumor cells undergoing epithelial-to-mesenchymal transition (EMT; cluster 10: *Krt8, Krt18, Sox9*, and loss of *Epcam*). In addition, cluster 8 was identified as stellate cells (*Rgs5, Col18a1*) (Figure 4a & Table S2).

Clusters 5, 7, 11, and 12 were identified as immune populations. As previously described, we confirmed that TGF-β1-blockade and chemo-immunotherapy induced enrichment in $CD8^+$ T cells, whereas Treg proportion was similar regardless of the TGF-β1 modulation (Figure 4b). Moreover, TGF-β1 could induce the M1/M2 polarization and the M1 macrophage cluster was only represented in samples with TGF-β1-blockade and chemo-immunotherapy (Figure 4c).

Within the remaining cells, different subpopulations of CAF were identified showing a heterogeneous distribution of this cell type (Clusters 0–4 and 6). Clusters 0, 3, and 4, were most abundant in samples treated by FOLFOX and PD-1/TGF-β1 dual inhibition (Figure 4a), suggesting that the CAF heterogeneity could be modulated by TGF-β1.

TGF-β1 inhibition dictates a chemokine switch in CAF subpopulations exposed to chemo-immunotherapy

To further assess the TGF-β1-mediated chemokine switch across this CAF heterogeneity, we compared the gene expression profiles modulated by TGF-β1 to the previously published CAF subtypes.[13,16] We reproduced myCAF and iCAF signatures using publicly available scRNA-seq data derived from KPC mice.[16] We applied these signatures to our dataset using the AUCell algorithm. myCAF population was highly represented in cluster 2, while clusters 0, 1, and 3 were strongly enriched by the iCAF signature (Figure 5a). Of note, the remaining CAF clusters (clusters 4 and 6) expressed both CAF signatures. Proliferating CAF (cluster 6) were characterized by the expression of mitotic markers such as *Mki67* and *Top2a* and a high number of detected genes (Figures 4a & S7A). Interestingly, the myCAF population from cluster 2 was restricted to cells of treated mice with chemo-immunotherapy; conversely, tumors exposed to anti-TGF-β1 therapy included mostly iCAF in clusters 0 and 3. Besides, cluster 1 included CAF derived from both treatment conditions (Figures 4a & 5a). All differentially expressed genes between cluster 2 (named myCAF) and cluster 0 (including mostly iCAF and cells derived from samples exposed to anti-TGF-β1) were summarized in Figure S7B and Table S3. The distribution of existing CAF markers[16,26,27] is depicted in Figure 5b. As previously described, myCAF/cluster 2 expressed high levels of *Acta2* [*αSMA], Postn* and *Lrrc15*[16,26] (Figure 5b). In contrast, *Pdgfra, Fap*, and *Pdpn* were predominantly expressed in iCAF clusters (Figure 5b). Albeit *Pdgfra* is associated with the iCAF signature,[16] these three genes are also described as pan-CAF markers. Here, all CAF clusters expressed pan-CAF markers including *Thy1* and *Col1a1* (data not shown). This first set of analyses indicated that TGF-β1 signaling promotes the organization of a myCAF-related TME, even when anti-PD-1 is combined with ICD-inducing chemotherapy.

The iCAF signature displayed enrichment in the cellular response to IFN-β/γ (FDR < .0001, NES = 30.3; and FDR = .004, NES = 10.3, respectively) including numerous cytokines (e.g., *Ifi203, Irf1, Ifi27l2a*), and expression of genes involved in antigen processing and presentation on MHC class I (Table S3 & Figure S7C). Also, the iCAF signature included inflammatory mediators, such as *Ly6c1*, as well as a plasminogen-kringle-4-binding protein, *Clec3b*, known to be secreted by CAF and promotes CRC[28] (Table S3). The myCAF signature was characterized by a strong enrichment in molecules regulating angiogenesis (FDR < .0001, NES = 11.3; including *Serpine1*), response to hypoxia (FDR < .0001, NES = 7.7; including *Cxcl12, Reg1*) and tumor necrosis factor (FDR = .0017, NES = 9.6; including *Il6, Sfrp1*), as well as cell chemotaxis (FDR < .0001, NES = 12.1; including *Cxcl14, Cxcl5*, and *Saa3*) (Table S3 & Figure S7C).

We next sought to explore the expression of chemokines within the different CAF subsets after therapy. As previously reported, iCAF were characterized by high enrichment of

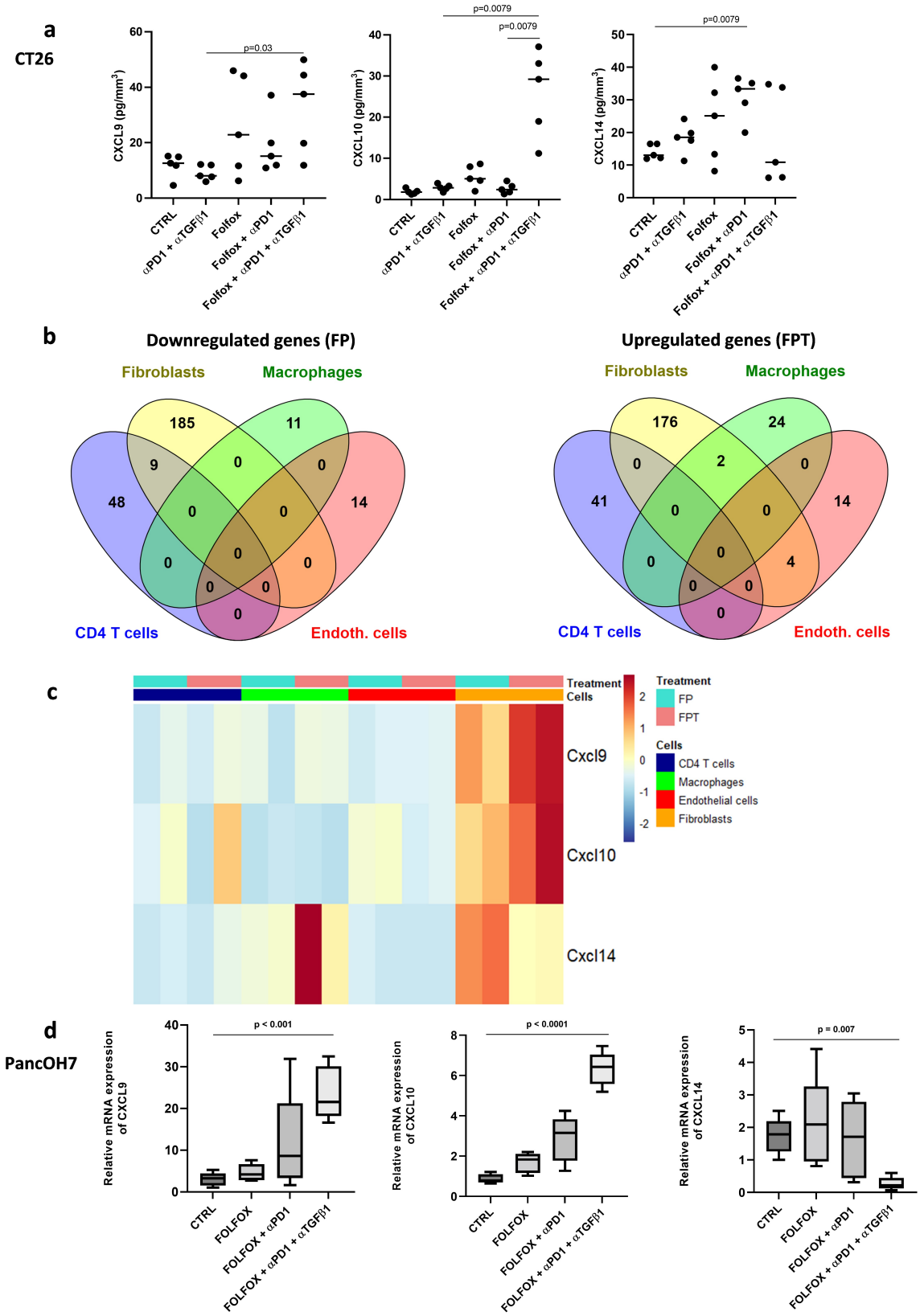

Figure 3. Anti-TGF-β1 combined with chemo-immunotherapy induces a chemokine switch in cancer-associated fibroblasts. (a) CXCL9, CXCL10, and CXCL14 levels determined in whole tumor lysate derived from the CT26 model and measured by ELISA. (b) Venn diagram showing overlaps between the transcriptomic signatures of $CD4^+$ T cells, macrophages, endothelial cells, and CAF isolated from CT26 tumor-bearing mice. Number of genes overexpressed with FP (Left) and FPT (Right) are represented. (c) Heatmap showing chemokine expression (z score) of cell sorted populations. (d) mRNA levels of CXCL9, CXCL10, and CXCL14 were determined by RT-qPCR in CAF from PancOH7 tumor-bearing mice. Housekeeping gene Glyceraldehyde-3-Phosphate Dehydrogenase (GAPDH) was uses for the normalization of data in RT-qPCR experiments. Abbreviations: CTRL: control; FP: FOLFOX+anti-PD-1; FPT: FOLFOX+anti-PD-1+ anti-TGF-β1.

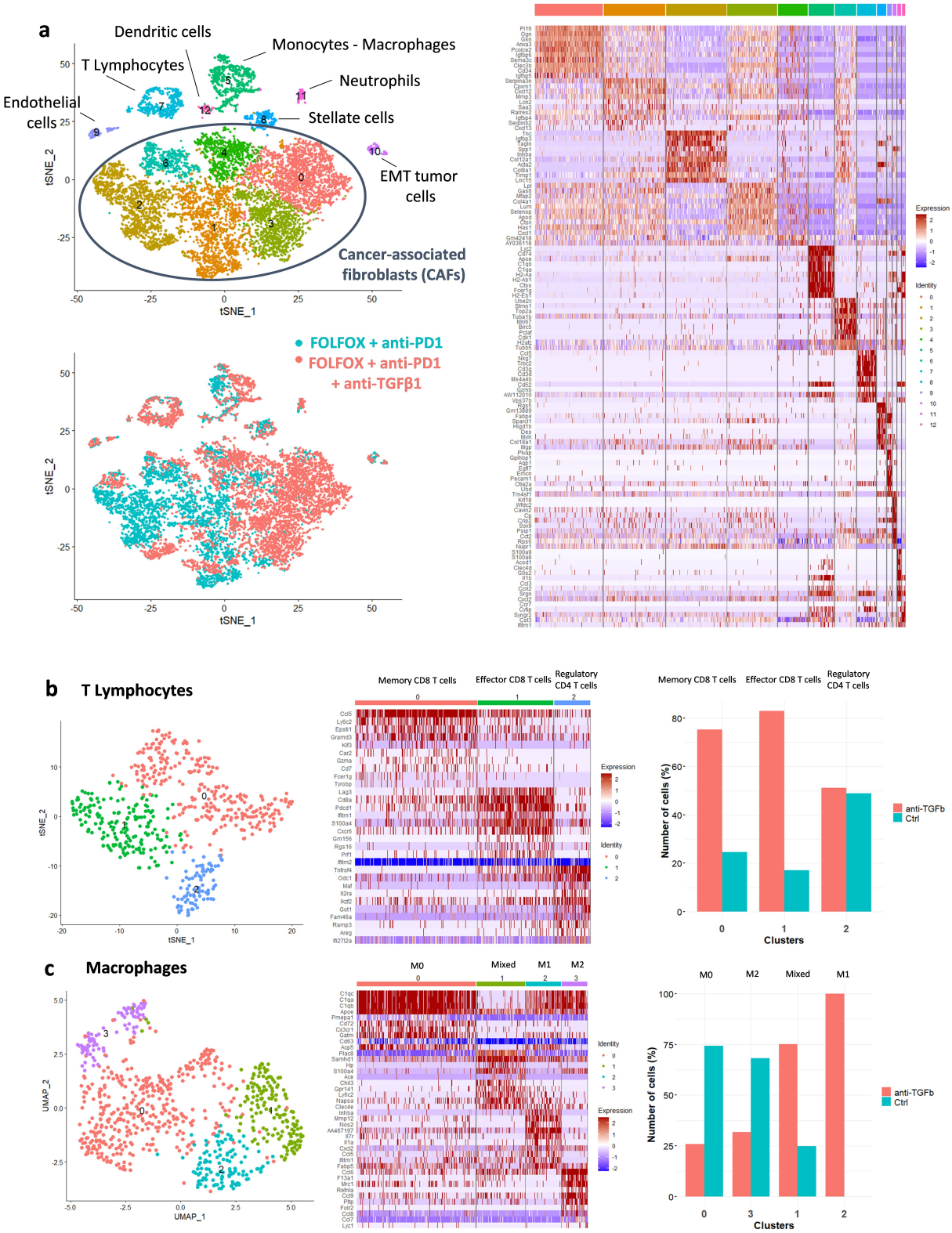

Figure 4. Cancer-associated fibroblast and immune cell heterogeneity after anti-TGF-β1 and chemo-immunotherapy combination at single-cell resolution. (a) t-distributed stochastic neighbor embedding (tSNE) embedding of 11,975 all single cells sorted from PancOH7 tumor-bearing C57BL/6 mice. Clusters identified through graph-clustering are indicated by color (Top left). Clusters across the two conditions of treatment (FOLFOX anti-PD-1 ± anti-TGF-β1; Bottom left). Heatmap showing the relative average expression of the most strongly enriched genes for each cluster; Top bars indicate clusters (Right). (b) tSNE embedding of T cells from cluster 7 in (A) (Left). Heatmap showing the relative average expression of the most strongly enriched genes for clusters from T cells. Three clusters of T cells were shown: t0, t1, and t2. High expression of genes associated with memory $CD8^+$ T cells in the t0 population (*Ccl5, Ly6c2*, and *Gzma*), while the t1 subset was characterized by markers of effector $CD8^+$ T cells (*Cd8a, Lag3, Pdcd1*, and *Prf1*). The transcriptional profile of the t2 population showed enrichment of regulatory $CD4^+$ T cell markers (*Tnfrsf4, Foxp3*, and *Cd4*). Proportion of T cells in each cluster according to treatment conditions (Right). (c) tSNE embedding of macrophages from cluster 5 in (A) (Left). Heatmap showing the relative average expression of the most strongly enriched genes for clusters from macrophages. Proportion of macrophages in each cluster according to treatment conditions (Right). Abbreviations: EMT: epithelial-to-mesenchymal transition.

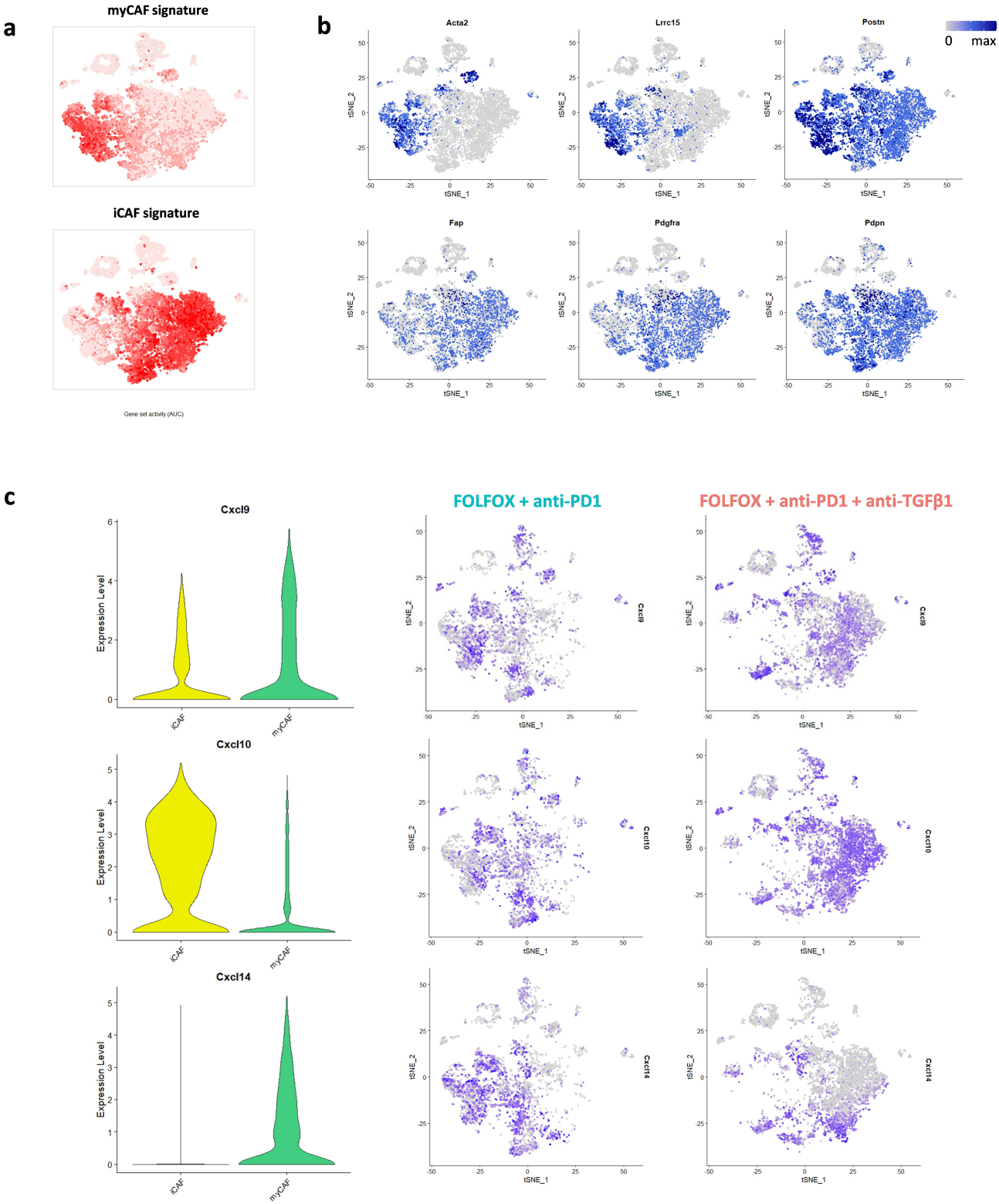

Figure 5. Chemokine switch across CAF subpopulations using single-cell RNA-sequencing. (a) AUCell-based tSNE representation coloring cells based on the gene set activities (AUC) of myCAF and iCAF signatures. (b) tSNEs illustrating the expression of the genes indicated in each panel. (c) Violin plots of expression of the indicated chemokines in myCAF and iCAF clusters (left). tSNEs illustrating the expression of the chemokines indicated in each panel split by treatment conditions (right).

immune chemoattractants.[16] Regarding Th1-type chemokines, we validated that *Cxcl10* was strongly expressed in the iCAF cluster. This observation was not confirmed for *Cxcl9* with a lower expression in cluster 0. In contrast, myCAF that clustered with our cluster 2, showed a low expression level for both CXCR3 ligands (Figure 5c). These modulations were also highlighted across treatment conditions, with a *Cxcl9/10* upregulation in cells exposed to chemo-immunotherapy and anti-TGF -β1, compared to cells in the absence of TGF-β1 inhibition (Figure 5c). As previously observed using bulk RNA-seq

(Figure 3), *Cxcl14* expression was decreased in CAF derived from PancOH7 and treated with chemo-immunotherapy and anti-TGF-β1 at the single-cell level (Figure 5c) supporting that TGF-β1-mediated activity on CAF contributes to the regulation of the chemokine switch required for chemo-immunotherapy efficacy. Similar results were observed and these signatures were validated in a second scRNA-seq executed with more mice (Figure S8).

The influence of TGF-β1 on CXCL9 and CXCL10 production by CAF is regulated by an epigenetic mechanism

We next decided to explore how TGF-β1 modulates the epigenetic regulation of CXCL9/10 in CAF. Normal fibroblasts, derived from naive mice, were exposed to TGF-β1 and/or IFNγ which triggers CXCL9/10 transcription. CXCL9/10 levels were significantly increased with IFNγ, but not with TGF-β1 alone. IFNγ-mediated chemokines expression was abrogated in the presence of TGF-β1 (Figures 6A-b).

G9a and EZH2 are two chromatin remodeling enzymes previously involved in the regulation of chemokine expression in cancer cells.[29,30] To elucidate if TGF-β1 also controls CXCL9/10 expression in CAF by epigenetic mechanisms, several epigenetic modulators were added in naive fibroblast cultures pretreated with TGF-β1. Normal fibroblasts were exposed for 72 hours to epigenetic therapies (UNC0638, GSKJ4, and GSK343) before treatment with IFNγ and chemokine production assessment. UNC0638 and GSK343 (inhibitors of histone methyltransferase: G9a and EZH2 inhibitors, respectively) were able to restore expression of CXCL9/10 in fibroblasts previously treated by TGF-β1, by contrast no modulation was shown after pre-treatment with GSKJ4 (inhibitor of H3K27me3-demethylases JMJD3/KDM6B and UTX/KDM6A: negative control; Figure 6b). This epigenetic therapy screening raised the hypothesis that G9a and EZH2 enzymes, targeted by UNC0638 and GSK343, control CXCR3 ligand expression. Inhibition of G9a or EZH2 leads to the removal of repressive H3K9me3 or H3K27me3, resulting in chromatin modification and CXCL9/10 gene re-expression in fibroblasts.[29,30] G9a and EZH2 inhibition, using chemical inhibitors or siRNA, restored CXCL9/10 expressions, preventing the effect of TGF-β1 on the epigenetic silencing of these chemokines (Figures 6c-d).

Although we could evidence an increased presence of permissive histone H3 acetylation at the CXCL10 promoter in fibroblast treated with TGF-β1 (Figure 6e), the repressive histone mark H3K9me3 was also enhanced at this promoter after treatment. Moreover, we profiled the chromatin accessibility landscape for CRC from TCGA database. A negative correlation between CXCL9 promoter ATAC-sequencing and a signature of genes induced by TGF-β1 (myCAF signature)[13,16] was observed ($R = -0.43$, $p = .0084$; figure 6f). Overall, these experiments revealed the role of G9a and EZH2 in the epigenetic regulation of TGF-β1-mediated chemokine expression in fibroblasts.

Discussion

Whether TGF-β1 remains an obstacle to ICI efficacy when immunotherapy is combined with chemotherapy is still elusive. Previous studies showed that TGF-β1 blockade enables cytotoxic lymphocyte homing in the tumor of mice treated with anti-PD-1.[1,2] Here, we first observed that TGF-β1 production remained detectable in tumors treated with ICD-inducing chemotherapy ± ICI. While TGF-β1 inhibition did not significantly potentiate the impact of FOLFOX chemotherapy, it was mandatory to achieve a high level of lymphocyte infiltration, as well as complete and durable remission in mice treated with FOLFOX+anti-PD-1. Therefore, TGF-β1 remains a potent immune-suppressive signaling impeding antigen-specific lymphocyte homing when ICD-inducing chemotherapy is combined with ICI.

Treg are widely reported to be a main source of TGF-β1 in the TME. Depleting Treg has previously been suggested as a possible strategy to enhance immune responses mediated by ICD.[3,31] Here, we observed that the level of Treg infiltration was further increased following chemo-immunotherapy treatment. However, the direct role of Treg in the modulation of ICD efficacy was ruled out since TGF-β1 neutralization was still effective in Treg-depleted mice. The precise role of Treg in TGF-β1-mediated resistance was previously interrogated in mouse tumors resistant to anti-PD-1. Treatment by anti-TGF-β1,2,3 or GARP:TGF-β1 neutralizing antibodies overcame resistance to PD-1/PD-L1 blockade. In these experiments, blocking TGF-β1 promoted antigen-specific $CD8^+$ T cell functions but did not increase the number of intra-tumoral specific T cells.[3] Conversely, we reported that adding TGF-β1 neutralizing agents to ICD-inducing chemotherapy enables the recruitment of $CD8^+$ T cells into the tumor.

Combining chemotherapy with ICI leveraged the production of CXCR3 ligands but also CXCL14 (Figure 3a). While TGF-β1 neutralization improved CXCL9/10 expression, it curtails the production of CXCL14 in responding tumors. Therefore, our results evidenced that the addition of TGF-β1 inhibitors to chemo-immunotherapy enabled a chemokine switch in the TME.

Using cell sorting, we also observed that CAF isolated from tumors exposed to chemo-immunotherapy ± TGF-β1 inhibitors produced more CXCL9/10/14 chemokines than endothelial cells, $CD4^+$ T lymphocytes, or macrophages. The potential role of CAF in this process was emphasized by the fact that TGF-β1 neutralization was not required for chemo-immunotherapy efficacy in $FAP^{-/-}$ mice (Figure S6). These results suggested that TGF-β1 suppression of ICD required the presence of CAF.

Several studies unraveled the presence of different CAF subsets in the cancer-associated stroma.[15,16] Notably, the presence of the myCAF subset was reported in tumors resistant to chemotherapy or immunotherapy.[26] The overall stromal composition of the cancer-related microenvironment was mostly described before treatment and the changes occurring in fibroblast heterogeneity exposed to chemo-immunotherapy were not thoroughly investigated. Our results showed that chemotherapy ± anti-PD-1 failed to decrease myCAF infiltration.

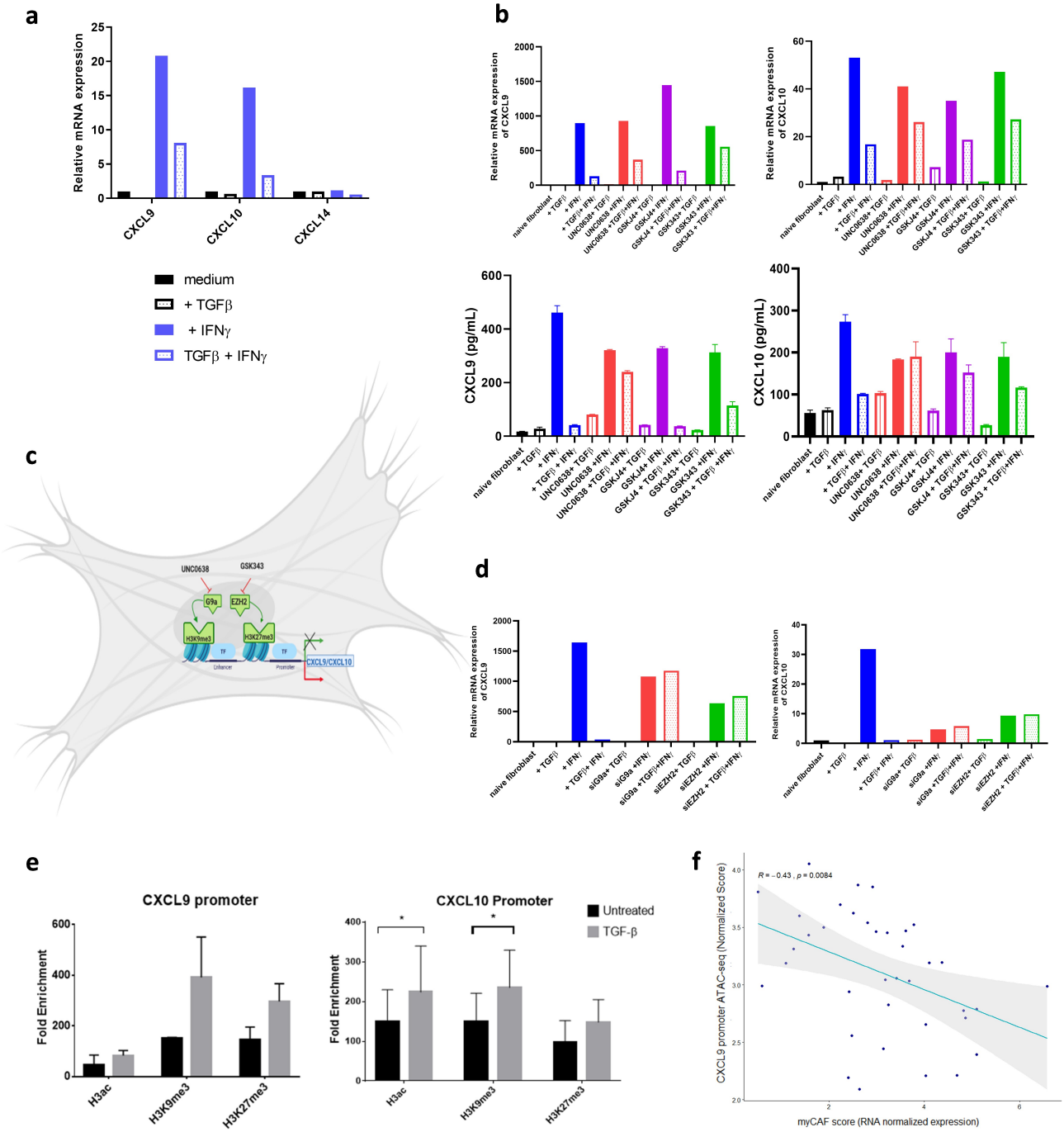

Figure 6. TGF-β1-induced epigenetic repression of CXCL9 and CXCL10 in fibroblasts is mediated by an interdependent cross-talk between EZH2 and G9a. (a) mRNA levels of CXCL9 and CXCL10 determined by RT-qPCR in naïve mouse fibroblasts (Left). CXCL9 and CXCL10 concentration in the medium analyzed by ELISA in the same fibroblasts (Right). Data are shown for one out of three representative experiments (b) mRNA levels of CXCL9 and CXCL10 determined by RT-qPCR in fibroblast incubated with epidrugs: EZH2 inhibitor (GSK343), G9a inhibitor (UNC0638), and JMJD3/KDM6B and UTX/KDM6A inhibitor (GSKJ4: negative control) (Top). CXCL9 and CXCL10 concentration in the medium analyzed by ELISA in the same conditions (Bottom). (c) Schematic representation of the interplay between EZH2 and G9a in the regulation of CXCL9/10 gene repression in naïve fibroblasts. (d) Naive mouse fibroblasts cells were transfected with control siRNA, EZH2 siRNA, or G9a siRNA in culture medium for 72 hours before incubation with TGF-β1 for 48 hours before being treated with IFNγ for a further 24 h. (e) Chromatin immunoprecipitation was conducted with specific antibodies against H3ac, H3K9me3, and H3K27me3 in confluent NIH/3T3 cells treated with TGF-β for 3 days and then fixed with formaldehyde. CXCL9 and CXCL10 promoters were amplified by qRT-PCR. Data are expressed as mean ± SEM of 2 or 3 separate experiments. *p < .05. (f) Correlation between CXCL9 promoter opening and myCAF signature in TCGA-COAD samples.

Similarly, only TGF-β1 neutralization allowed recruitment and differentiation of iCAF after chemo-immunotherapy.

Assessing the heterogeneity of CAF subpopulations during treatment in humans is technically challenging. Therefore, we selected two reproducible mouse models allowing the early tumor sampling in satellite groups, to better evaluate the impact of chemo-immunotherapy on CAF recruitment. A limitation of these syngeneic murine models was linked to the analysis of small tumors more representative of the metastasis initiation stage. A validation with large tumors or

genetically engineered mouse models might be warranted. Besides, CAF subsets could vary between mice and humans. However, previous studies confirm the stability of myCAF and iCAF phenotypes through species.[13,16]

While myCAF produced high levels of CXCL14 in mice exposed to FOLFOX+anti-PD-1, iCAF produced increased levels of Th1-type chemokines and lower CXCL14 when TGF-β1 inhibitors were added to ICD-inducing chemotherapy.

Previous investigations have also evidenced the heterogeneity of iCAF isolated from breast cancers. Interestingly, the CXCL9/10 CAF signature observed in CAF isolated from tumors exposed to chemo-immunotherapy and TGF-β1 inhibitors was similar to the gene expression profile of the "IFN-iCAF" cluster.[17] Above CXCR3 ligand expression modulation, our results showed that TGF-β1 neutralization also prevents expression of CXCL14 in most iCAF, while high levels of this chemokine were still observed in tumors from mice treated with FOLFOX and anti-PD-1 combination (Figure 3a).

While paradoxical effects of CXCL14 overexpression are observed in cancer cells,[32,33] high stromal CXCL14 expression was significantly associated with a poor prognosis.[34] CXCL14-expressing fibroblasts could enhance the growth of prostate cancer xenografts, trigger tumor angiogenesis and macrophage recruitment, and enhance monocyte migration, through NOS1-derived nitric oxide signaling.[35,36] Albeit no specific receptor has been identified, ACKR2 mediates CXCL14-induced downstream NOS1 activation to initiate EMT programs and enhance the cancer-promoting functions of fibroblasts.[37] Thus, CXCL14 might constitute a potential drug target for the management of cancer.

CXCL14, as well as CXCL12, promotes idiopathic pulmonary fibrosis through CXCR4.[38] Of note, a CXCR4 antagonist (BL-8040) in combination with chemo-immunotherapy induced an ORR of 32% in patients with metastatic PDAC.[39] This association also increased $CD8^+$ effector T cell tumor infiltration and decreased circulating Treg. CXCL9/10 are upregulated by cytokine stimulation in cancer cells, monocytes, endothelial cells, as well as in CAF.[40–42] Reprogramming CAF gene expression in order to restore CXCL9/10 expression could also be an attractive approach to promote ICI efficacy. Recent data from preclinical studies support this strategy, particularly through NOX4 inhibition.[43] An epigenetic reprogramming may predominantly target the expression of these chemokines[30] and contribute to immunotherapy resistance. In our study, G9a and EZH2 were identified as the targeted enzymes by UNC0638 and GSK343, respectively, preventing the effect of TGF-β1 on the induction of CXCL9/10 in CAF. Other epigenetic factors than those associated with TGF-β1 have been implicated in CXCL9 transcriptional regulation, such as LIF.[14,44] In addition, hypomethylation-mediated activation of IRX1 positively regulates CXCL14/NF-κB signaling to promote metastatic activities in osteosarcoma.[45] However, ACKR2, NOX4, and IRX1 are not correlated with CXCL9/10/14 expression in CAF from our experiments (data not shown).

Our results provide evidence that G9a and EZH2 contribute to the immune evasion mediated by CAF and that chemical targeting of these histone methyl-transferases might reprogram the chemokine production profile. Recent reports sustain the potential of G9a and EZH2 dual inhibition as an attractive approach to reinvigorate cancer immunity. Indeed, Spiliopoulou *et al* showed that dual G9a and EZH2 inhibition acts directly on tumor cells to modulate chemokine expression profile and to restore the expression of ERV-K endogenous retroviral elements as a source of tumor-associated antigens.[46]

Altogether, our results show that TGF-β1 remains an important immune suppressive pathway when ICD-chemotherapy is combined with ICI. TGF-β1 signaling drives the constitution of a myCAF-enriched tumor microenvironment in mice treated by chemo-immunotherapy and prevents accessibility of CXCL9/10 promoters in a G9a and EZH2-dependent fashion.

Acknowledgments

This work was supported by grants from the Ligue contre le cancer du grand Est, the Cancéropôle Est, and from Région Bourgogne Franche-Comté. We thank the Institute of Genetics and Molecular and Cellular Biology (Ilkirch, France) for technical assistance.

Disclosure statement

CB declares research grant from Roche, Bayer and advisory board for MSD, Sanofi, Bayer. All other authors report no conflict of interest.

Funding

The author(s) reported there is no funding associated with the work featured in this article.

Authors' contributions

CB conceived the study. JRP performed animal studies, bulk RNA-seq, flow cytometry, ELISA, and RT-qPCR. AV, JRP, AB performed single-cell RNA-seq. ER, EH, PP performed epigenetic analyses. AV performed statistical and bioinformatic analyses. AV, JRP, ER, JV, AB, LS, MK, SA, RL, EH, PP, CB analyzed the data. AV, JRP, CB wrote the manuscript.

References

1. Mariathasan S, Turley SJ, Nickles D, Castiglioni A, Yuen K, Wang Y, Kadel III EE, Koeppen H, Astarita JL, Cubas R, *et al*. TGFβ attenuates tumour response to PD-L1 blockade by contributing to exclusion of T cells. Nature. 2018;554(7693):544–548. doi:10.1038/nature25501.
2. Tauriello DVF, Palomo-Ponce S, Stork D, Berenguer-Llergo A, Badia-Ramentol J, Iglesias M, Sevillano M, Ibiza S, Cañellas A, Hernando-Momblona X, *et al*. TGFβ drives immune evasion in genetically reconstituted colon cancer metastasis. Nature. 2018;554(7693):538–543. doi:10.1038/nature25492.
3. de Streel G, Bertrand C, Chalon N, Liénart S, Bricard O, Lecomte S, Devreux J, Gaignage M, De Boeck G, Mariën L, *et al*. Selective inhibition of TGF-β1 produced by GARP-expressing Tregs overcomes resistance to PD-1/PD-L1 blockade in cancer. Nat Commun. 2020;11(1):4545. doi:10.1038/s41467-020-17811-3.
4. Strauss J, Heery CR, Schlom J, Madan RA, Cao L, Kang Z, Lamping E, Marté JL, Donahue RN, Grenga I, *et al*. Phase I Trial of M7824 (MSB0011359C), a Bifunctional Fusion Protein Targeting PD-L1 and TGFβ, in Advanced Solid Tumors. Clin Cancer Res. 2018;24(6):1287–1295. doi:10.1158/1078-0432.CCR-17-2653.
5. Kang Y-K, Bang Y-J, Kondo S, Chung HC, Muro K, Dussault I, Helwig C, Osada M, Doi T. Safety and Tolerability of Bintrafusp Alfa, a Bifunctional Fusion Protein Targeting TGFβ and PD-L1, in

Asian Patients with Pretreated Recurrent or Refractory Gastric Cancer. Clinical Cancer Research. 2020;26(13):3202–3210. doi:10.1158/1078-0432.CCR-19-3806.
6. Pfirschke C, Engblom C, Rickelt S, Cortez-Retamozo V, Garris C, Pucci F, Yamazaki T, Poirier-Colame V, Newton A, Redouane Y, *et al*. Immunogenic Chemotherapy Sensitizes Tumors to Checkpoint Blockade Therapy. Immunity. 2016;44(2):343–354. doi:10.1016/j.immuni.2015.11.024.
7. Dosset M, Vargas TR, Lagrange A, Boidot R, Végran F, Roussey A, Chalmin F, Dondaine L, Paul C, Marie-Joseph EL, *et al*. PD-1/PD-L1 pathway: an adaptive immune resistance mechanism to immunogenic chemotherapy in colorectal cancer. Oncoimmunology. 2018;7(6):e1433981. doi:10.1080/2162402X.2018.1433981.
8. Galluzzi L, Buqué A, Kepp O, Zitvogel L, Kroemer G. Immunological Effects of Conventional Chemotherapy and Targeted Anticancer Agents. Cancer Cell. 2015;28(6):690–714. doi:10.1016/j.ccell.2015.10.012.
9. Tesniere A, Schlemmer F, Boige V, Kepp O, Martins I, Ghiringhelli F, Aymeric L, Michaud M, Apetoh L, Barault L, *et al*. Immunogenic death of colon cancer cells treated with oxaliplatin. Oncogene. 2010;29(4):482–491. doi:10.1038/onc.2009.356.
10. Calon A, Lonardo E, Berenguer-Llergo A, Espinet E, Hernando-Momblona X, Iglesias M, Sevillano M, Palomo-Ponce S, Tauriello DVF, Byrom D, *et al*. Stromal gene expression defines poor-prognosis subtypes in colorectal cancer. Nat Genet. 2015;47(4):320–329. doi:10.1038/ng.3225.
11. Guinney J, Dienstmann R, Wang X, de Reyniès A, Schlicker A, Soneson C, Marisa L, Roepman P, Nyamundanda G, Angelino P, *et al*. The consensus molecular subtypes of colorectal cancer. Nat Med. 2015;21(11):1350–1356. doi:10.1038/nm.3967.
12. Chakravarthy A, Khan L, Bensler NP, Bose P, De Carvalho DD. TGF-β-associated extracellular matrix genes link cancer-associated fibroblasts to immune evasion and immunotherapy failure. Nat Commun. 2018;9(1). doi:10.1038/s41467-018-06654-8.
13. Öhlund D, Handly-Santana A, Biffi G, Elyada E, Almeid AS, Ponz-Sarvis M, Corbo V, Oni TE, Hearn SA, Lee EJ, *et al*. Distinct populations of inflammatory fibroblasts and myofibroblasts in pancreatic cancer. J Exp Med. 2017;214:579–596. doi:10.1084/jem.20162024.
14. Biffi G, Oni TE, Spielman B, Hao Y, Elyada E, Park Y, Preall J, Tuveson DA. IL1-Induced JAK/STAT Signaling Is Antagonized by TGFβ to Shape CAF Heterogeneity in Pancreatic Ductal Adenocarcinoma. Cancer Discov. 2019;9(2):282–301. doi:10.1158/2159-8290.CD-18-0710.
15. Costa A, Kieffer Y, Scholer-Dahirel A, Pelon F, Bourachot B, Cardon M, Sirven P, Magagna I, Fuhrmann L, Bernard C, *et al*. Fibroblast Heterogeneity and Immunosuppressive Environment in Human Breast Cancer. Cancer Cell. 2018;33(3):463–479.e10. doi:10.1016/j.ccell.2018.01.011.
16. Elyada E, Bolisetty M, Laise P, Flynn WF, Courtois ET, Burkhart RA, Teinor JA, Belleau P, Biffi G, Lucito MS, *et al*. Cross-Species Single-Cell Analysis of Pancreatic Ductal Adenocarcinoma Reveals Antigen-Presenting Cancer-Associated Fibroblasts. Cancer Discov. 2019;9(8):1102–1123. doi:10.1158/2159-8290.CD-19-0094.
17. Kieffer Y, Hocine HR, Gentric G, Pelon F, Bernard C, Bourachot B, Lameiras S, Albergante L, Bonneau C, Guyard A, *et al*. Single-cell analysis reveals fibroblast clusters linked to immunotherapy resistance in cancer. Cancer Discov. 2020;10(9):1330–1351. doi:10.1158/2159-8290.CD-19-1384.
18. Chen Y, Kim J, Yang S, Wang H, Wu C-J, Sugimoto H, LeBleu VS, Kalluri R. Type I collagen deletion in αSMA+ myofibroblasts augments immune suppression and accelerates progression of pancreatic cancer. Cancer Cell. 2021;39(4):548–565.e6. doi:10.1016/j.ccell.2021.02.007.
19. Chow MT, Ozga AJ, Servis RL, Frederick DT, Lo JA, Fisher DE, Freeman GJ, Boland GM, Luster AD. Intratumoral Activity of the CXCR3 Chemokine System Is Required for the Efficacy of Anti-PD-1 Therapy. Immunity. 2019;50(6):1498–1512.e5. doi:10.1016/j.immuni.2019.04.010.
20. Grauel AL, Nguyen B, Ruddy D, Laszewski T, Schwartz S, Chang J, Chen J, Piquet M, Pelletier M, Yan Z, *et al*. TGFβ-blockade uncovers stromal plasticity in tumors by revealing the existence of a subset of interferon-licensed fibroblasts. Nature Communications. 2020;11(1):6315. doi:10.1038/s41467-020-19920-5.
21. Zhang D, Qiu X, Li J, Zheng S, Li L, Zhao H. TGF-β secreted by tumor-associated macrophages promotes proliferation and invasion of colorectal cancer via miR-34a-VEGF axis. Cell Cycle Georget Tex. 2018;17(24):2766–2778. doi:10.1080/15384101.2018.1556064.
22. Zagozda M, Sarnecka AK, Staszczak Z, Nowak-Niezgoda M, Durlik M. Correlation of TNF-α and TGF-β polymorphisms with protein levels in pancreatic ductal adenocarcinoma and colorectal cancer. Contemp Oncol Poznan Pol. 2019;23:214–219.
23. Castle JC, Loewer M, Boegel S, de Graaf J, Bender C, Tadmor AD, Boisguerin V, Bukur T, Sorn P, Paret C, *et al*. Immunomic, genomic and transcriptomic characterization of CT26 colorectal carcinoma. BMC Genom. 2014;15(1):190. doi:10.1186/1471-2164-15-190.
24. Romero JM, Grünwald B, Jang GH, Bavi PP, Jhaveri A, Masoomian M, Fischer SE, Zhang A, Denroche RE, Lungu IM, *et al*. A Four-Chemokine Signature Is Associated with a T-cell-Inflamed Phenotype in Primary and Metastatic Pancreatic Cancer. Clin Cancer Res. 2020;26:1997–2010. doi:10.1158/1078-0432.CCR-19-2803.
25. Lu J, Chatterjee M, Schmid H, Beck S, Gawaz M. CXCL14 as an emerging immune and inflammatory modulator. J Inflamm Lond Engl. 2016;13:1.
26. Dominguez CX, Muller S, Keerthivasan S, Koeppen H, Hung J, Gierke S, Breart B, Foreman O, Bainbridge TW, Castiglioni A, *et al*. Single-cell RNA sequencing reveals stromal evolution into LRRC15 + myofibroblasts as a determinant of patient response to cancer immunotherapy. Cancer Discov. 2019. doi:10.1158/2159-8290.CD-19-0644.
27. Neuzillet C, Tijeras-Raballand A, Ragulan C, Cros J, Patil Y, Martinet M, Erkan M, Kleeff J, Wilson J, Apte M, *et al*. Inter- and intra-tumoural heterogeneity in cancer-associated fibroblasts of human pancreatic ductal adenocarcinoma. J Pathol. 2019;248(1):51–65. doi:10.1002/path.5224.
28. Zhu H-F, Zhang X-H, Gu C-S, Zhong Y, Long T, Ma Y-D, Hu Z-Y, Li Z-G, Wang X-Y. Cancer-associated fibroblasts promote colorectal cancer progression by secreting CLEC3B. Cancer Biol Ther. 2019;20(7):967–978. doi:10.1080/15384047.2019.1591122.
29. Coward WR, Brand OJ, Pasini A, Jenkins G, Knox AJ. Interplay between EZH2 and G9a Regulates CXCL10 Gene Repression in Idiopathic Pulmonary Fibrosis. Am J Respir Cell Mol Biol. 2018;58(4):449–460. doi:10.1165/rcmb.2017-0286OC.
30. Peng D, Kryczek I, Nagarsheth N, Zhao L, Wei S, Wang W, Sun Y, Zhao E, Vatan L, Szeliga W, *et al*. Epigenetic silencing of TH1-type chemokines shapes tumour immunity and immunotherapy. Nature. 2015;527(7577):249–253. doi:10.1038/nature15520.
31. Kalathil S, Lugade AA, Miller A, Iyer R, Thanavala Y. Higher frequencies of GARP(+)CTLA-4(+)Foxp3(+) T regulatory cells and myeloid-derived suppressor cells in hepatocellular carcinoma patients are associated with impaired T-cell functionality. Cancer Res. 2013;73:2435–2444. doi:10.1158/0008-5472.CAN-12-3381.
32. Hata R-I, Izukuri K, Kato Y, Sasaki S, Mukaida N, Maehata Y, Miyamoto C, Akasaka T, Yang X, Nagashima Y, *et al*. Suppressed rate of carcinogenesis and decreases in tumour volume and lung metastasis in CXCL14/BRAK transgenic mice. Sci Rep. 2015;5(1):9083. doi:10.1038/srep09083.
33. Wang Y, Weng X, Wang L, Hao M, Li Y, Hou L, Liang Y, Wu T, Yao M, Lin G, *et al*. HIC1 deletion promotes breast cancer progression by activating tumor cell/fibroblast crosstalk. Journal of Clinical Investigation. 2018;128(12):5235–5250. doi:10.1172/JCI99974.

34. Sjöberg E, Augsten M, Bergh J, Jirström K, Östman A. Expression of the chemokine CXCL14 in the tumour stroma is an independent marker of survival in breast cancer. Br J Cancer. 2016;114:1117–1124. doi:10.1038/bjc.2016.104.
35. Augsten M, Hägglöf C, Olsson E, Stolz C, Tsagozis P, Levchenko T, Frederick MJ, Borg Å, Micke P, Egevad L, *et al*. CXCL14 is an autocrine growth factor for fibroblasts and acts as a multi-modal stimulator of prostate tumor growth. Proc Natl Acad Sci U S A. 2009;106(9):3414–3419. doi:10.1073/pnas.0813144106.
36. Augsten M, Sjöberg E, Frings O, Vorrink SU, Frijhoff J, Olsson E, Borg Å, Östman A. Cancer-associated fibroblasts expressing CXCL14 rely upon NOS1-derived nitric oxide signaling for their tumor-supporting properties. Cancer Res. 2014;74(11):2999–3010. doi:10.1158/0008-5472.CAN-13-2740.
37. Sjöberg E, Meyrath M, Milde L, Herrera M, Lövrot J, Hägerstrand D, Frings O, Bartish M, Rolny C, Sonnhammer E, *et al*. A Novel ACKR2-Dependent Role of Fibroblast-Derived CXCL14 in Epithelial-to-Mesenchymal Transition and Metastasis of Breast Cancer. Clin Cancer Res. 2019;25(12):3702–3717. doi:10.1158/1078-0432.CCR-18-1294.
38. Rodriguez LR, Emblom-Callahan M, Chhina M, Bui S, Aljeburry B, Tran LH, Novak R, Lemma M, Nathan SD, Grant GM, *et al*. Global Gene Expression Analysis in an in vitro Fibroblast Model of Idiopathic Pulmonary Fibrosis Reveals Potential Role for CXCL14/CXCR4. Scientific Reports. 2018;8(1):3983. doi:10.1038/s41598-018-21889-7.
39. Bockorny B, Semenisty V, Macarulla T, Borazanci E, Wolpin BM, Stemmer SM, Golan T, Geva R, Borad MJ, Pedersen KS, *et al*. BL-8040, a CXCR4 antagonist, in combination with pembrolizumab and chemotherapy for pancreatic cancer: the COMBAT trial. Nat Med. 2020;26(6):878–885. doi:10.1038/s41591-020-0880-x.
40. House IG, Savas P, Lai J, Chen AXY, Oliver AJ, Teo ZL, Todd KL, Henderson MA, Giuffrida L, Petley EV, *et al*. Macrophage-Derived CXCL9 and CXCL10 Are Required for Antitumor Immune Responses Following Immune Checkpoint Blockade. Clin Cancer Res. 2020;26:487–504. doi:10.1158/1078-0432.CCR-19-1868.
41. Kistner L, Doll D, Holtorf A, Nitsche U, Janssen K-P. Interferon-inducible CXC-chemokines are crucial immune modulators and survival predictors in colorectal cancer. Oncotarget. 2017;8(52):89998–90012. doi:10.18632/oncotarget.21286.
42. Tokunaga R, Zhang W, Naseem M, Puccini A, Berger MD, Soni S, McSkane M, Baba H, Lenz H-J. CXCL9, CXCL10, CXCL11/CXCR3 axis for immune activation - A target for novel cancer therapy. Cancer Treat Rev. 2018;63:40–47. doi:10.1016/j.ctrv.2017.11.007.
43. Ford K, Hanley CJ, Mellone M, Szyndralewiez C, Heitz F, Wiesel P, Wood O, Machado M, Lopez M-A, Ganesan A-P, *et al*. NOX4 Inhibition Potentiates Immunotherapy by Overcoming Cancer-Associated Fibroblast-Mediated CD8 T-cell Exclusion from Tumors. Cancer Res. 2020;80(9):1846–1860. doi:10.1158/0008-5472.CAN-19-3158.
44. Pascual-García M, Bonfill-Teixidor E, Planas-Rigol E, Rubio-Perez C, Iurlaro R, Arias A, Cuartas I, Sala-Hojman A, Escudero L, Martínez-Ricarte F, *et al*. LIF regulates CXCL9 in tumor-associated macrophages and prevents CD8+ T cell tumor-infiltration impairing anti-PD1 therapy. Nat Commun. 2019;10(1):2416. doi:10.1038/s41467-019-10369-9.
45. Lu J, Song G, Tang Q, Zou C, Han F, Zhao Z, Yong B, Yin J, Xu H, Xie X, *et al*. IRX1 hypomethylation promotes osteosarcoma metastasis via induction of CXCL14/NF-κB signaling. J Clin Invest. 2015;125(5):1839–1856. doi:10.1172/JCI78437.
46. Spiliopoulou P, Spear S, Mirza H, Garner I, McGarry L, Grundland-Freile F, Cheng Z, Ennis DP, Iyer N, McNamara S, *et al*. Dual G9A/EZH2 Inhibition Stimulates Antitumor Immune Response in Ovarian High-Grade Serous Carcinoma. Mol Cancer Ther. 2022;21(4):522–534. doi:10.1158/1535-7163.MCT-21-0743.